Available online at www.sciencedirect.com
ScienceDirect
Trans. Nonferrous Met. Soc. China 34(2024) 80−93
Transactions of Nonferrous Metals Society of China
www.tnmsc.cn

Effect of ultrasonic vibration on microstructures and mechanical properties of friction stir welded 2195 Al−Li alloy

Xiang DAI[1], Lei SHI[1], Chun-yan TIAN[1], Chuan-song WU[1], Song GAO[2]

1. Key Laboratory for Liquid−Solid Structure Evolution and Processing of Materials, Ministry of Education, Shandong University, Jinan 250061, China;
2. School of Mechanical Engineering, Qilu University of Technology (Shandong Academy of Sciences), Jinan 250353, China

Received 17 June 2022; accepted 20 September 2022

Abstract: A novel ultrasonic vibration enhanced friction stir welding (UVeFSW) was employed to join the third-generation 2195-T6 Al−Li alloy, and the effect of ultrasonic vibration on microstructures and mechanical properties of the joint was studied. It is revealed that UVeFSW can enhance the plastic material flow to suppress the weld defects. The critical welding speed of sound joints is increased in UVeFSW compared with conventional FSW. When ensuring that the tensile strength of the joint is 75% that of the base material, the welding speed and efficiency in UVeFSW are higher than those in conventional FSW. Superimposing ultrasonic vibration can significantly enhance the mechanical properties of 2195 Al−Li alloy FSW joints at a higher welding speed. The maximum tensile strength of the UVeFSW joint is 449.5 MPa, which is 83.1% that of the base material. UVeFSW can increase the welding efficiency by increasing the critical welding speed and simultaneously ensuring the joint properties.

Key words: 2195-T6 Al−Li alloy; friction stir welding; ultrasonic vibration enhanced friction stir welding; welding speed; grain structure; joint properties

1 Introduction

The third-generation Al−Li alloy possesses high specific strength and specific stiffness, good corrosion resistance and excellent low-temperature fatigue performance, which shows a promising application in the aerospace industry [1−3]. Replacing conventional aerospace aluminium alloys with Al−Li alloy can reduce the weight of structural parts by more than 15% and increase the stiffness by more than 10%. Therefore, it has become one of the primary lightweight structural materials in the aerospace industry [1,2]. However, traditional fusion welding is hardly possible to obtain an excellent joint since hot cracks, welding porosity and even the evaporation loss of Li elements are very easy to occur, which seriously reduces the performance of joints and affects the reliability of structural parts [3]. Friction stir welding (FSW) is a solid-phase joining technology [4−7], which has become one of the preferred welding methods for light metals [8−11]. FSW possesses the advantages of low welding temperature and low welding distortion, which makes it possible to avoid the main drawbacks introduced in conventional fusion welding [12−15].

Many researchers have carried out friction stir welding of 2195 Al−Li alloy to explore its welding possibility [16−20]. FONDA et al [21] used the "emergency stop" method when friction stir welding 2195 Al−Li alloy plates with a thickness of

Corresponding author: Lei SHI, Tel/Fax: +86-531-88395987, E-mail: lei.shi@sdu.edu.cn
DOI: 10.1016/S1003-6326(23)66383-6

25 mm, and used the electron back-scattered diffraction (EBSD) technique to observe the evolution of the grain structure. They found that a large number of rotational shear textures appear in the thermo-mechanically affected zone (TMAZ) at the advancing side (AS), and the main grain refinement mechanisms in this region are deformation and dynamic recovery. TAYON et al [22] studied the texture in the TMAZ of 2195 Al−Li alloy FSW joints and revealed that a large number of low Taylor factor grains contributed to the fracture of joint at the TMAZ. WU et al [23] carried out friction stir welding of 2195-T8 plates with a thickness of 7.5 mm and achieved the highest tensile strength of FSW joints, which is 70% that of the base metal. SHUKLA and BAESLACK [24] studied distribution characteristic of precipitates in different regions of 2195-T8 Al−Li alloy FSW joint. They found that the θ' (Al_2Cu) phase was completely dissolved into the matrix in the weld nugget zone (WNZ), while the length of the T_1 (Al_2CuLi) phase was reduced and part of the θ' phase was coarsened in the heat-affected zone. QIN et al [25] studied the precipitation phase of the 2195-T8 Al−Li alloy FSW joint with a thickness of 5 mm and found that significant softening occurs in the WNZ of the FSW joints.

As FSW relies mainly on the frictional and plastic deformation heat generation between the welding tool and the workpiece to plasticize the material, which results in a larger welding force and limits the critical welding speed for sound joints to a relatively low value [26−29]. To overcome these shortcomings of the conventional FSW process, various variant FSW technologies with auxiliary energy fields have been proposed [30−33]. Ultrasonic vibration energy, as a kind of mechanical energy, possesses the advantage of reducing the plastic deformation resistance of metal materials without increasing the welding temperature. Therefore, superimposing ultrasonic vibration in FSW is a promising method to overcome the shortcomings of the conventional FSW [32]. TARASOV et al [34] proposed an ultrasonic-assisted FSW process by using an extended backing plate to support the plate to be welded and connecting the ultrasonic vibration tool to the extended end of the backing plate through bolts. They conducted ultrasonic-assisted friction stir welding of 2195 Al−Li alloy by using this equipment and found that the application of ultrasonic vibration reduced the grain size and promoted the formation of the precipitates in the WNZ. HU et al [35] studied the effect of ultrasonic vibration on the recrystallization process and precipitation behaviour of 2060-T8 Al−Li alloy FSW joints with a thickness of 2 mm. It was revealed that the application of ultrasonic vibration shortens the incubation time of dynamic recrystallization and lowers the activation threshold of plastic deformation for dynamic recrystallization, as well as promotes the reprecipitation of nanoscale precipitates. ELISEEV et al [36] studied the effect of ultrasonic vibration on the microstructure of 2195 Al−Li alloy FSW joint with a thickness of 1.8 mm. They found that the application of ultrasonic vibration increased the deformation of the joint material, which results in a larger number of T_1 phase precipitates in the WNZ. It is evident that there is a little preheating effect in the ultrasonic energy assisted FSW compared with other external energy assisted FSW. Therefore, superimposing ultrasonic vibration energy in FSW is promising in controlling the heat transfer and plastic deformation to improve joint properties in the friction stir welded Al−Li alloy joints. However, the influence of superimposing ultrasonic vibration in FSW on the microstructure and properties of Al−Li alloy friction stir welded joints is still unrevealed.

In this work, the application potential of the novel ultrasonic vibration enhanced FSW (UVeFSW) process was explored in welding third-generation Al−Li alloys. The underlying mechanism of ultrasonic vibration on the microstructures and mechanical properties of friction stir welded 2195 Al−Li alloy was studied. This can provide experimental data and theoretical support for the realization of high-quality and high-efficiency joining of the third-generation Al−Li alloys.

2 Experimental

The as-received AA2195-T6 sheets with a thickness of 2.0 mm were friction stir welded parallel to the rolling direction in a butt joint configuration. The chemical composition of the base material (BM) is given in Table 1. The schematic of UVeFSW is shown in Fig. 1. In the

UVeFSW process, an ultrasonic tool with a hemispheric endpoint was placed ahead of the FSW tool at a distance of 20 mm. The ultrasonic vibration tool was inclined by 40° with respect to the top surface of the workpiece. The amplitude of the ultrasonic vibration was 40 μm. The ultrasonic frequency and the output power of ultrasonic vibration were 20 kHz and 300 W, respectively.

Table 1 Chemical composition of 2195 Al−Li alloy (wt.%)

Cu	Li	Mg	Ag	Zr	Fe	Ti	Al
4.01	1.02	0.52	0.29	0.11	≤0.15	≤0.15	Bal.

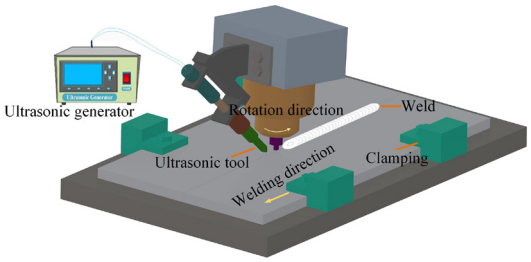

Fig. 1 Schematic drawing of ultrasonic vibration enhanced friction stir welding (UVeFSW)

A tapered tool was employed in the welding process. The details of the tool dimensions and features are given in Table 2. The tool used for this work was made of H13 tool steel, as shown in Fig. 2(a). It consisted of a 2° concave shoulder with a diameter of 8 mm and a tapered tool pin with right-hand thread. The thread pitch of the tool pin was 0.36 mm. The length of the pin was 1.8 mm. The diameter of the tool pin was 3.2 mm at the root, while it was 2.2 mm at the tip. A tilt angle of 2.5° was chosen for the tool during the welding process. The plunge depth of the tool shoulder was 0.15 mm. The surface of the welding region was polished with sandpapers to remove the oxide layer and then cleaned up with acetone before welding. During welding, the FSW tool rotated in the counter-clockwise direction. The welding parameters used in this study are listed in Table 3. The welding speeds investigated varied between 60 and 570 mm/min at a constant rotation speed of 600 r/min.

After welding, joints were cut perpendicular to the welding direction using an electrical-discharge cutting machine. The dimensions for tensile test samples are shown in Fig. 2(b). The tensile test samples were polished with sandpapers to remove the cutting edges. Then, tensile tests were conducted at a constant loading velocity of 1 mm/min using a WDW−100AE universal testing machine. The fracture surfaces of tensile samples were observed using a JSM−7800F field emission scanning electron microscope (FE-SEM). The microhardness of each area of the joint was measured using an automatic turret Vickers hardness tester (type HVS−1000Z−W) at 0.5, 1 and 1.5 mm from the upper surface of the weld with a load of 2.94 N and a holding time of 10 s.

Table 2 Tool geometry

Tool geometry	Feature or dimension
Shoulder diameter/mm	8
Shoulder type	Concave
Pin length/mm	1.8
Pin root diameter/mm	3.2
Pin tip diameter/mm	2.2
Pin type	Conical with screw thread

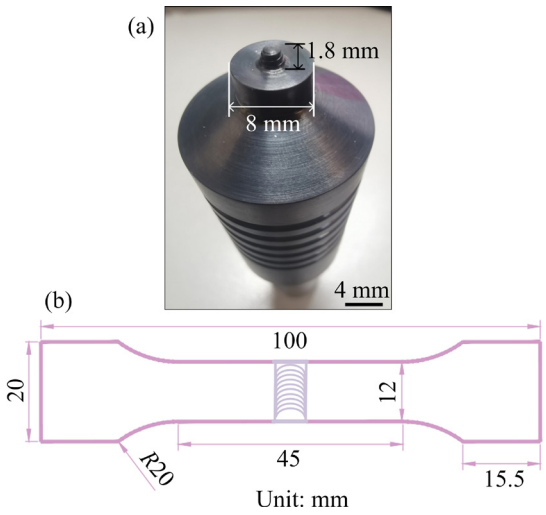

Fig. 2 Appearance of welding tool (a) and dimensions of tensile sample (b)

Table 3 Process parameters

Tool rotational speed/(r·min^{-1})	Weld speed/ (mm·min^{-1})	Depth of penetration/mm	Tool tilt angle/(°)
600	60−570	0.15	2.5

The metallographic samples were prepared and etched using Keller's reagent (2.5 mL HNO_3 + 1.5 mL HCl + 1 mL HF + 95 mL H_2O) and examined by optical microscopy. The samples used

for electron backscatter diffraction (EBSD) were mechanically polished and then electropolished using a solution of 15% perchloric acid and 85% ethanol at −20 °C under a potential of 15 V for 12 s. The corresponding EBSD maps were generated using JSM−7800F FE-SEM equipped with a NordlysMax3 EBSD system. The inverse pole figure (IPF), grain boundary distribution and micro-texture (pole figures) were obtained and analyzed by HKL−CHANNEL 5 software.

3 Results and discussion

3.1 Effect of ultrasonic vibration on weld macro-structures

Figure 3 shows the macroscopic metallography of the weld cross-section at a welding speed of 570 mm/min for both conventional FSW and UVeFSW. It is shown that the volume of WNZ for the UVeFSW is larger than that for conventional FSW. In addition, a joint line remnant defect (i.e., zig-zag line) is seen in the conventional FSW joint. This is due to the fact that the low welding temperature at a relatively high welding speed of 570 mm/min would lead to less plastic deformation and stirring during the conventional FSW process, resulting in a joint line remnant defect [9]. However, no joint line remnant defect is observed in the UVeFSW joint. This is mainly because the acoustic softening enhances the plastic deformation in the WNZ during the UVeFSW process, which helps break the oxidation film at the joint interface.

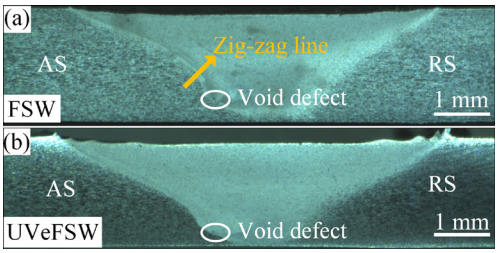

Fig. 3 Cross-sectional morphologies of 2195-T6 joints obtained at welding speed of 570 mm/min: (a) FSW; (b) UVeFSW (AS−Advancing side; RS−Retreating side)

Furthermore, a small void defect occurs at the AS of the WNZ for both conventional FSW and UVeFSW. The corresponding enlarged images of void defects for both conventional FSW and UVeFSW joints are shown in Fig. 4. Compared to the conventional FSW, the void defects in the UVeFSW joint is smaller and closer to the bottom of the weld. This is mainly due to the fact that the acoustic softening effect of ultrasonic vibration energy reduces the flow stress of the plastic material near the tool, which enhances the plastic material flow and makes it easier to flow downwards, resulting in a smaller void defect in the UVeFSW joint closer to the bottom of the weld. Another noteworthy phenomenon is that the boundary between the TMAZ and WNZ penetrates into the WNZ resulting in a bulge of the interface at the AS in conventional FSW joint, while the boundary between the TMAZ and WNZ at the AS in UVeFSW is smooth. This phenomenon is a consequence of better plastic material flow in the WNZ with superimposing ultrasonic vibration in the UVeFSW process.

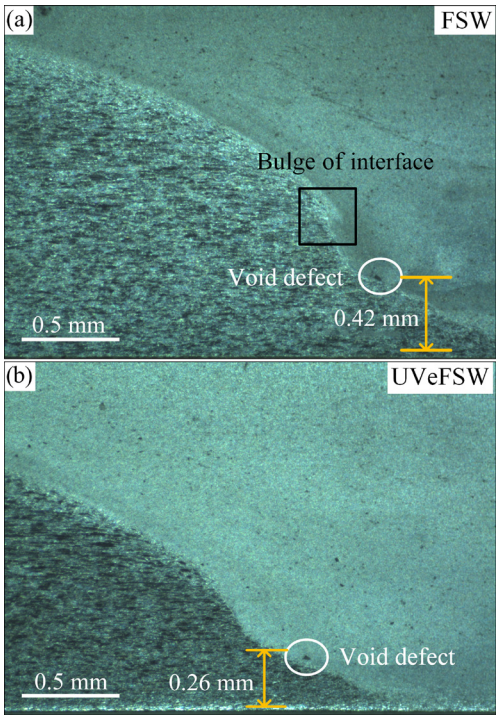

Fig. 4 Local morphologies of 2195-T6 joints obtained at welding speed of 570 mm/min: (a) FSW; (b) UVeFSW

To quantitatively analyze the influence of superimposing ultrasonic vibration energy on the weld formation, the weld cross-section at the welding speed of 120 mm/min was observed using a metallurgical microscope, as shown in Fig. 5. It can be seen that sound welds with no defect are achieved at the welding speed of 120 mm/min in both conventional FSW and UVeFSW. Similar features of the cross-section of the weld are observed

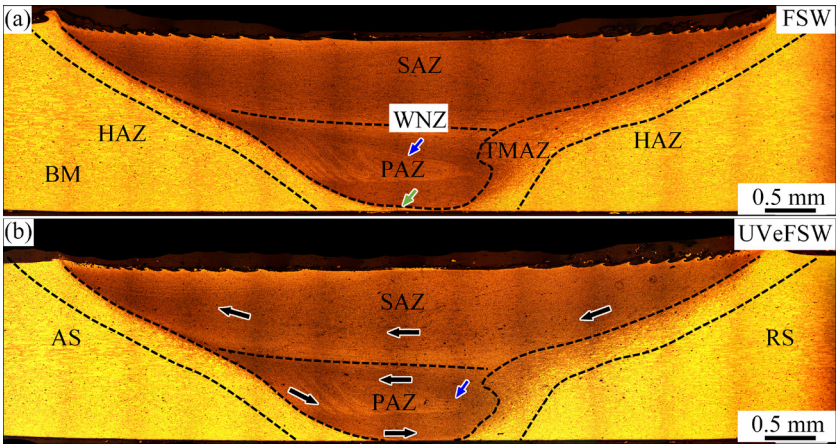

Fig. 5 Morphologies of 2195-T6 joints obtained at welding speed of 120 mm/min: (a) FSW; (b) UVeFSW

for both conventional FSW and UVeFSW. Each weld can be divided into the WNZ, TMAZ, heat affected zone (HAZ) and BM. In addition, the WNZ can be further subdivided into the shoulder-affected zone (SAZ) and pin-affected zone (PAZ), depending on deformation characteristics of the material. As can be seen from Fig. 5, the shear direction of the plastic materials in the WNZ is schematically represented by the black arrow. Since the tool with right-hand thread is tilted backward and rotates in a counterclockwise direction, it is evident that the plastic material in the SAZ near the boundary of WNZ flows downward under the stirring effect of the shoulder.

Furthermore, the plastic material in the PAZ near the boundary of WNZ at the AS flows downward and then moves to the retreating side (RS), while the plastic materials at the RS flow upward and in contact with the downward plastic material flow driven by the tool shoulder, and then change its flow direction. The TMAZ on the RS penetrates into the WNZ which increases the maximum width of the TMAZ on the RS. The onion ring (shown by the blue arrow in Fig. 5) appears in the PAZ for both the conventional FSW and UVeFSW, which is attributed to the cyclical material flow within the WNZ [37,38]. In addition, a small region at the bottom of the conventional FSW joint shows the similar microstructures of TMAZ (shown by the green arrows in Fig. 5), while fully plastic deformation occurs at the bottom of the UVeFSW joint resulting in the similar microstructures of the WNZ. This indicates that superimposing ultrasonic vibration energy promotes the plastic material flow and enhances the recrystallization process of the plastic material at the bottom of the WNZ in the UVeFSW.

The width of the WNZ at different depths from the top surface of the workpiece in Fig. 5 is measured and listed in Table 4. It can be seen that the width of the WNZ in UVeFSW at different depths is larger than that in the conventional FSW. It is distinct that the width of the WNZ at the depth of 1.0 mm from the top surface of the workpiece (i.e., in the middle of the weld) is increased from 3.48 mm in the conventional FSW to 4.29 mm in the UVeFSW. SHI et al [39] proposed an integrated UVeFSW model and revealed that the coupling of ultrasonic vibration energy with the plastically deformed material in front of the tool pre-softens the plastic material, which leads to lower flow stress and enhanced plastic material flow in the WNZ. As a result, the volume of the WNZ in the UVeFSW is increased compared with that in conventional FSW.

Table 4 Width of WNZ at different depths at welding speed of 120 mm/min

Distance from top surface/mm	Width of WNZ/mm	
	FSW	UVeFSW
0.5	6.2	6.4
1.0	3.5	4.3
1.5	2.5	2.6

3.2 Effect of ultrasonic vibration on weld microstructures

3.2.1 Grain structures

To analyze the typical grain characteristics of the friction stir welded 2195 Al−Li alloy joints,

high-resolution EBSD was carried out on the typical areas of FSW joints at the welding speed of 120 mm/min. Figure 6(a) shows the EBSD map of the WNZ with the TMAZ at the AS, while Fig. 6(b) shows the EBSD map of the TMAZ at the RS. There are mainly refined and recrystallized grains in the WNZ, while medium-sized deformed grains are observed in the TMAZ due to the dynamic recovery. By comparing Fig. 6(a) with Fig. 6(b), it can be found that the boundary between TMAZ and WNZ at AS of the weld is clearer than that at RS. This is because the material at AS experiences severe shear deformation under the stirring of the tool resulting in a severe dynamic recrystallization process [40], and the newly formed refined recrystallized grains are significantly different from the partially deformed grains in the TMAZ. However, the plastic materials near the boundary between the WNZ and TMAZ at the RS mainly experience an extrusion process with a lower strain rate. Therefore, the grain structure in the WNZ at the RS is similar to that in the TMAZ. Figure 6(c) shows that the grain structure in the HAZ is similar to that of the parent material (Fig. 6(d)) dominated by (001) and (111) crystal orientations. The EBSD map of HAZ shows the morphology of the originally rolled grains with larger grain sizes. The average grain diameter for HAZ is 11.5 μm which is larger than that of 9.7 μm for the parent material, as shown in Fig. 6(d).

Since both the conventional FSW and UVeFSW joint were fractured at the WNZ, to investigate the effect of superimposing ultrasonic vibration field on the grain size, morphology and orientation in the WNZ, high-resolution EBSD was carried out for both conventional FSW and UVeFSW in the middle of WNZ at the welding speed of 120 mm/min. Figure 7 depicts that a large number of refined and recrystallized equiaxed grains are distributed in the WNZ for both the conventional FSW and UVeFSW. The average grain size in the middle of the WNZ of the FSW joint is 1.01 μm, while the average grain size is slightly reduced to 0.98 μm in the WNZ of the UVeFSW joint. This indicates that the superimposing ultrasonic energy in FSW does not lead to severe grain growth in the WNZ, because the acousto-plastic effect of ultrasonic energy reduces the flow

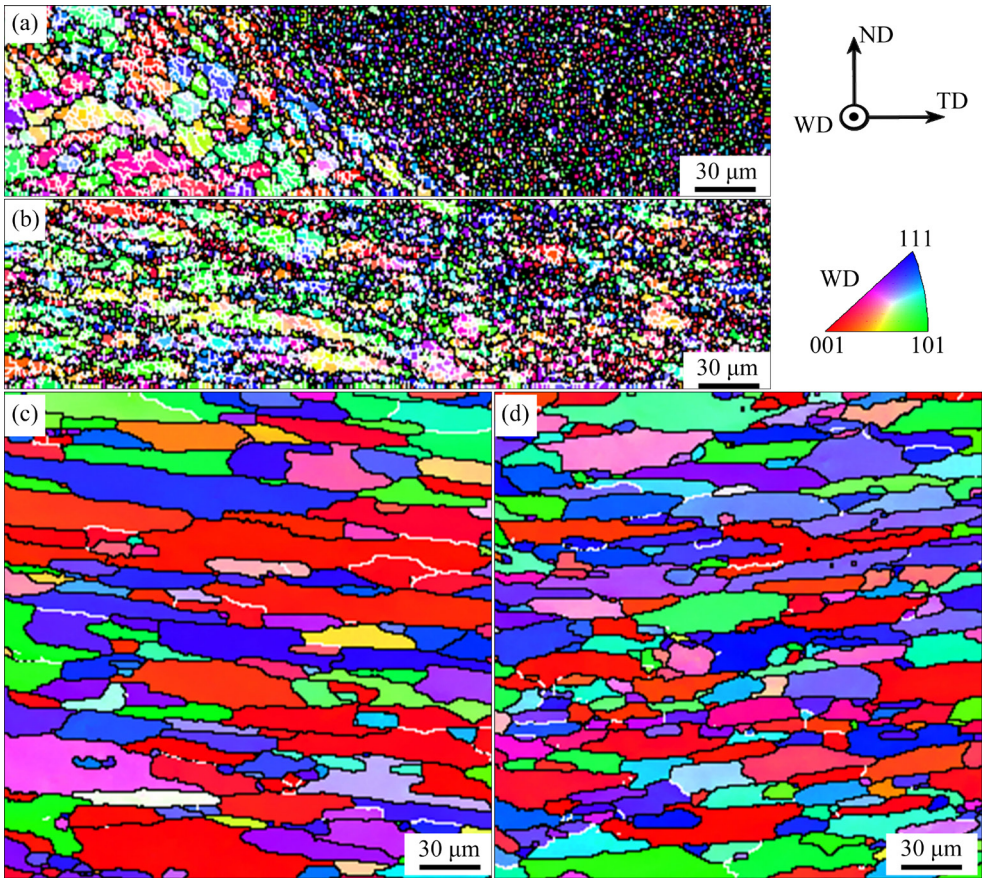

Fig. 6 High-resolution EBSD maps of FSW joints at welding speed of 120 mm/min: (a) AS-TMAZ; (b) RS-TMAZ; (c) HAZ; (d) BM

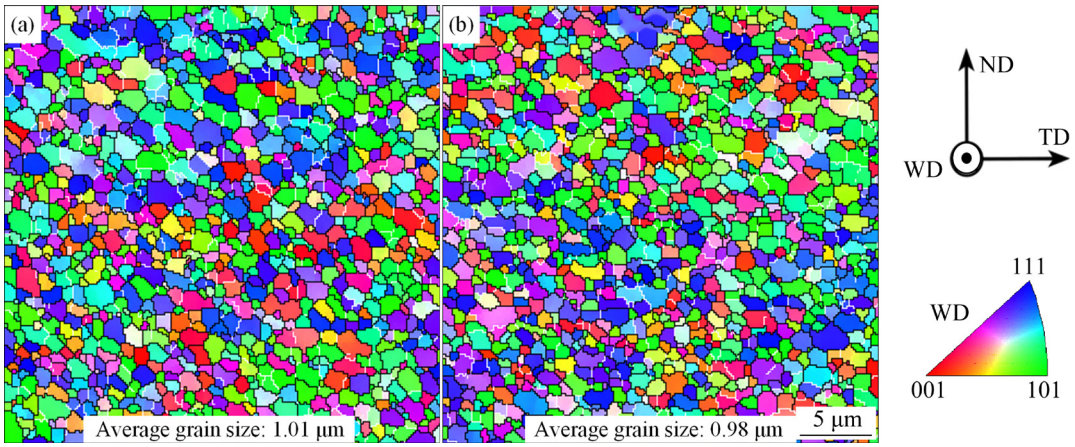

Fig. 7 High-resolution EBSD maps of WNZ at welding speed of 120 mm/min: (a) FSW; (b) UVeFSW

stress of the plastic materials in the WNZ, which lowers the plastic deformation heat generation while enhancing the plastic deformation in the WNZ. The severe plastic deformation can enhance the recrystallization process in the WNZ. Therefore, similar fine grain is achieved in the WNZ of the UVeFSW joint compared with the conventional FSW joint.

Figure 8 shows the grain boundary map, misorientation distribution map and recrystallized grain distribution map in the middle of the WNZ for both conventional FSW and UVeFSW joints at the welding speed of 120 mm/min. It is depicted that the proportions of high-angle grain boundaries in the middle of the WNZ for conventional FSW and UVeFSW are both higher than 80%. This is because the high heat input and severe plastic deformation in the WNZ facilitate the dynamic recovery and dynamic recrystallization process. Therefore, the low-angle grain boundaries are transformed into high-angle grain boundaries through the absorption of dislocations [41]. Furthermore, the proportion of high-angle grain boundaries in the middle of the WNZ of conventional FSW joints is 81.6% which is lower than that of UVeFSW joints. In addition, the proportion of recrystallized grain for conventional FSW is 71.7%, while it is increased to 81.4% when superimposing ultrasonic vibration in the UVeFSW process. This is because the ultrasonic vibration energy enhances the plastic material flow, shortens the incubation time of dynamic recrystallization and lowers the activation threshold of plastic deformation for dynamic recrystallization, which promotes the dislocation motion in the WNZ resulting in a higher proportion of recrystallized grains in the middle of the WNZ for UVeFSW joint [34,42].

3.2.2 Micro-textures

Micro-texture represents preferred grain orientation in a representative micro-area of material. The pole figure is a stereographic projection of the grain orientations and intensities. To investigate the influence of superimposing ultrasonic vibration on the micro-texture of joint, the micro-texture analysis was carried out by the pole figures of the WNZ for both FSW and UVeFSW, as shown in Fig. 9. It is illustrated that the recrystallization texture appears in the WNZ of conventional FSW and UVeFSW. This is because the grain structure in the WNZ experiences severe plastic deformation. Furthermore, partial grains with the deformed texture still retain the preferred orientation after dynamic recovery and dynamic recrystallization. It is revealed that there is mainly recrystallization texture with the presence of $\{110\}\langle 110\rangle$ components. In addition, the fiber texture with the presence of $\langle 110\rangle$//TD components, as well as partial C texture with the presence of $\{001\}\langle 110\rangle$ components are also observed in the WNZ. It is noteworthy that the textures in both FSW and UVeFSW are strong and similar and the maximum peak intensity achieved is ~5 times random. It is indicated that superimposing ultrasonic vibration in FSW has little influence on the type and maximum intensity of micro-texture of friction stir welded 2195 Al−Li alloy, which is consistent with previous experimental results for conventional aerospace aluminum alloy [43,44].

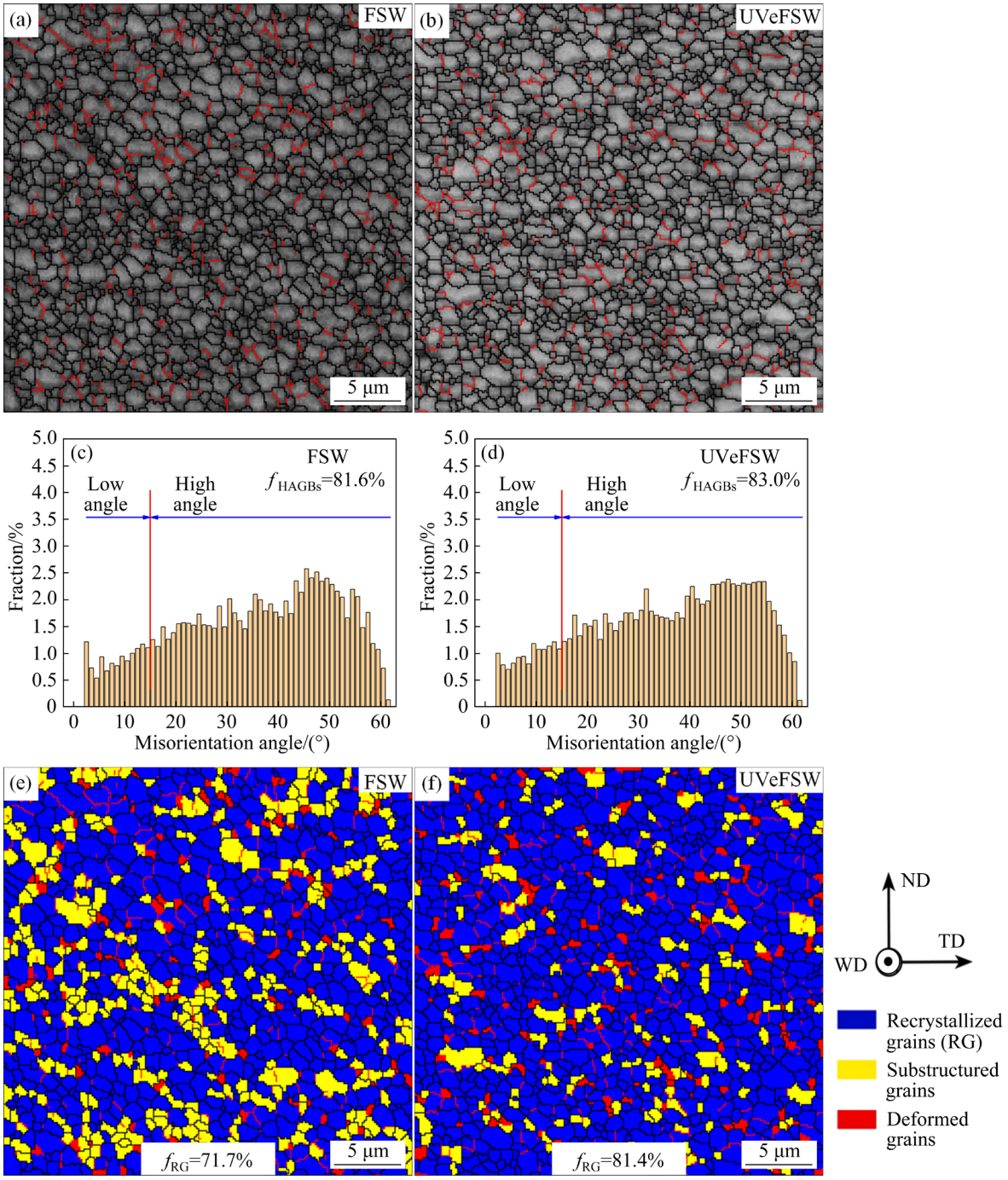

Fig. 8 Grain boundary maps (a, b), misorientation angle distributions (c, d) and recrystallization maps (e, f) in middle of WNZ at welding speed of 120 mm/min: (a, c, e) FSW; (b, d, f) UVeFSW

3.3 Effect of ultrasonic vibration on mechanical properties

3.3.1 Tensile properties

Figure 10 compares the tensile properties of FSW and UVeFSW joints at different welding speeds. As is observed in Fig. 10(a), the ultimate tensile strength of the joints increases by increasing the welding speed from 60 to 120 mm/min and then decreases by further increasing the welding speed to 570 mm/min. The maximum ultimate tensile strength of the conventional FSW joint is 445.8 MPa which is achieved at the welding speed of 120 mm/min, while the maximum ultimate tensile strength of the UVeFSW joint is 449.5 MPa (83.1% that of the base material) which is slightly higher than that of the conventional FSW process.

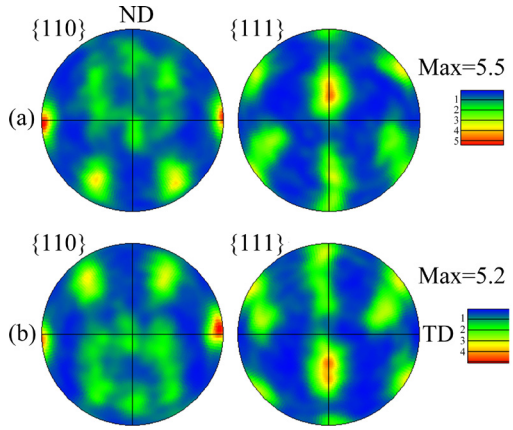

Fig. 9 {110} and {111} pole figures in middle of WNZ at welding speed of 120 mm/min for conventional FSW (a) and UVeFSW (b)

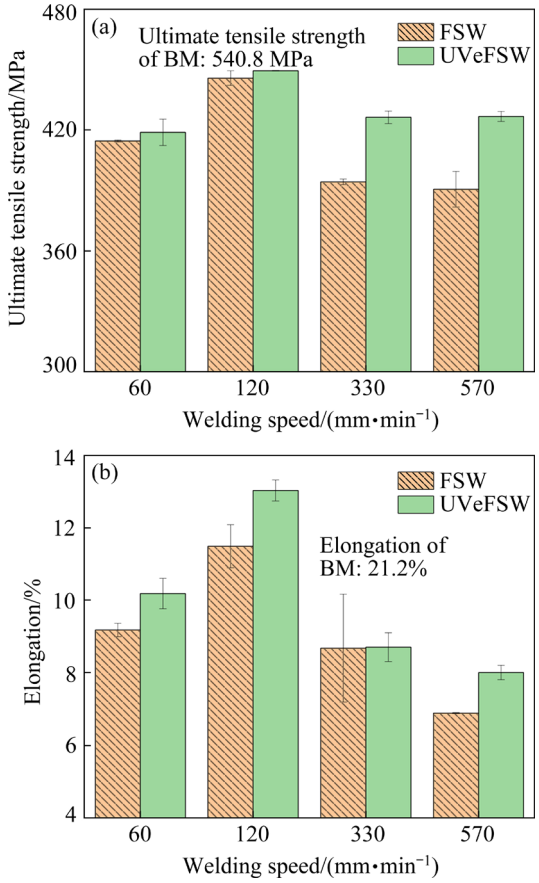

Fig. 10 Tensile test results: (a) Ultimate tensile strength; (b) Elongation

Furthermore, the ultimate tensile strength of the conventional FSW joints at the welding speed of 570 mm/min is 390.7 MPa, while it increases to 426.8 MPa when superimposing the ultrasonic vibration in the UVeFSW. This indicates that superimposing ultrasonic vibration can significantly enhance the joint properties, especially at a high welding speed, due to a better acoustic softening effect at the lower welding temperature [45]. Figure 10(b) depicts the elongation of both FSW and UVeFSW joints at different welding speeds. It is shown that the elongation increases with an increase of the welding speed from 60 to 120 mm/min, and then it decreases with further increasing the welding speed. The elongation of the UVeFSW joints at different welding speeds is larger than that of the conventional FSW joints with the same welding parameter. For industry application, the tensile strength of the joint is usually required to be 75% that of base material (i.e., 405.6 MPa). It is evident that tensile strength of conventional FSW joint at the welding speed of 330 mm/min is 394.4 MPa, which is lower than 75% that of the base material. However, the tensile strength of the UVeFSW joint at the welding speed of 570 mm/min is 426.8 MPa, which is about 79% that of the base material. Thus, superimposing ultrasonic vibration in FSW can significantly increase the critical welding speed and welding efficiency, as well as ensure the requirement of joint properties for industry application.

3.3.2 Microhardness

Figure 11 shows the hardness distribution profiles on the cross-section of both conventional FSW and UVeFSW joints at the welding speed of 120 mm/min. Figures 11(a−c) represent the hardness distribution profiles at a depth of 0.5 mm (top), 1.0 mm (middle) and 1.5 mm (bottom) from the top surface of the weld, respectively. It is depictd that the geometry of all microhardness distribution profiles of the joints is in a typical W shape, which is always related to the four distinct zones of the joint (i.e., WNZ, TMAZ, HAZ and BM). The BM possesses the highest hardness with a hardness value of HV 178, while the microhardness in the other zones of the joints is decreased compared to the BM as significant thermal softening occurs. This softening phenomenon of the joint is caused by different microstructural evolutions in various zones which is a typical characteristic of FSW of Al−Li alloys [25]. The minimum hardness is located in the HAZ, mainly due to the coarsening and dissolution of the precipitated phase in the HAZ under the influence of the welding thermal cycle [7], as well as the coarsening of the grain. In addition, it can be seen that the hardness of the WNZ in the upper part of

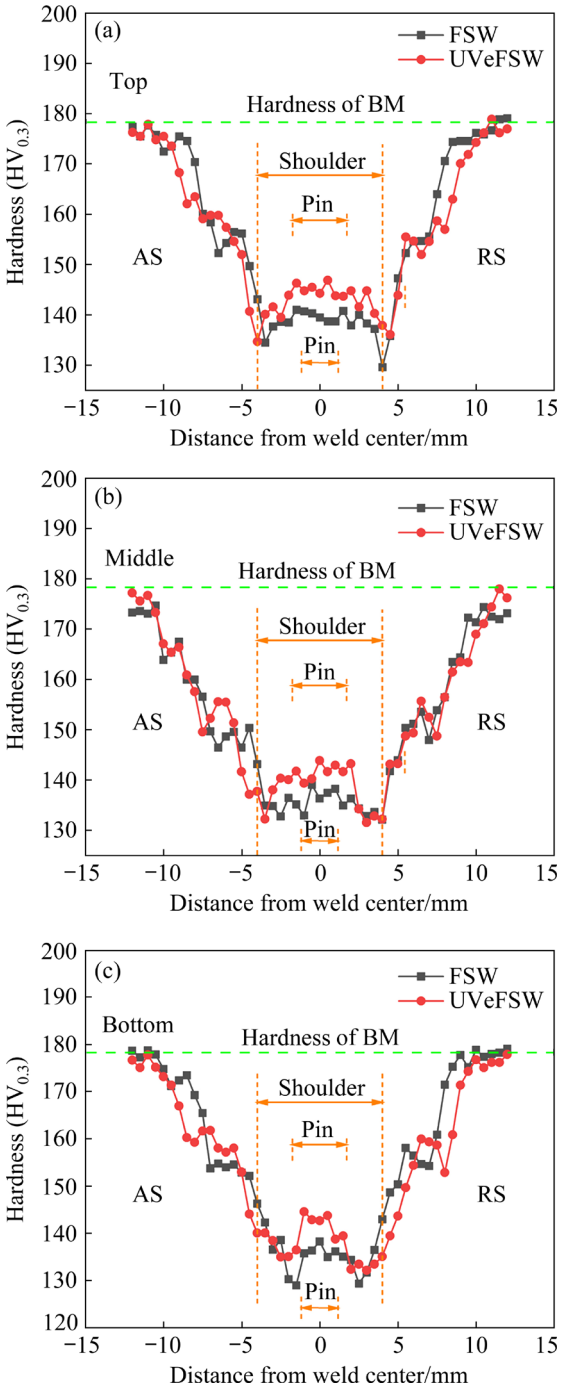

Fig. 11 Micro-hardness profiles of FSW and UVeFSW joints at welding speed of 120 mm/min and different depths from top surface of workpiece: (a) 0.5 mm; (b) 1.0 mm; (c) 1.5 mm

the weld (Fig. 11(a)) is higher than that in the middle and bottom of the weld (Figs. 11(b, c)). This is because the materials in the upper part of the weld experience a higher peak temperature and longer high-temperature dwell time which facilitate the nucleation and growth of the precipitated phase, resulting in a higher hardness value. Comparing the hardness profiles of conventional FSW with the UVeFSW joints (Fig. 11) illustrates that the value of hardness in the WNZ of UVeFSW is higher than that in conventional FSW. This indicates that superimposing ultrasonic vibration in FSW can increase the hardness value of the WNZ of the joint since ultrasonic vibration energy promotes the formation of precipitates [35], which in turn improves the hardness of the WNZ of the joint. In addition, superimposing ultrasonic vibration in FSW enhances the plastic material flow, which increases the width of the WNZ and reduces the width of the HAZ. Therefore, the part with the lowest joint hardness is located further away from the center of the weld, and the minimum hardness of the UVeFSW joint is slightly higher than that of the conventional FSW joint.

3.3.3 Fracture features

Figure 12 shows the fracture locations of joints obtained by conventional FSW and UVeFSW at the welding speed of 120 mm/min. It is depicted that both the conventional FSW and UVeFSW joints are fractured in the WNZ. The relatively low welding heat input results in an incompletely recrystallized region at the bottom of the WNZ for the FSW joint (Fig. 5(a)), which leads to a crack initiating at the bottom of the WNZ. As a result, the conventional FSW joint fractures in the middle of the WNZ. However, superimposing ultrasonic vibration in the FSW enhances the plastic deformation and suppresses the formation of an incompletely recrystallized region at the bottom of the WNZ for the UVeFSW joint. Therefore, the crack initiates at the boundary of TMAZ and WNZ and then expands to the WNZ for the UVeFSW joint.

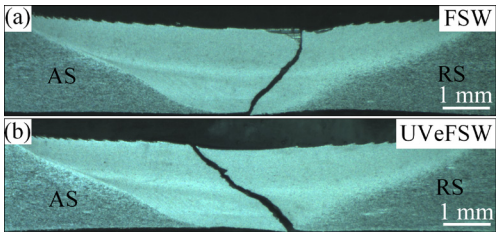

Fig. 12 Fracture locations of joints at welding speed of 120 mm/min: (a) FSW; (b) UVeFSW

Characteristics on the fracture surface are the direct manifestation of the fracture feature of these tensile specimens. To clarify the fracture feature

in detail and further illustrate the effect of superimposing ultrasonic vibration on the tensile properties of the joints, the fracture morphologies of conventional FSW and UVeFSW joints at the welding speed of 120 mm/min were analyzed and compared. Figure 13 shows fracture morphology of the conventional FSW joint. It can be seen that there are many small and shallow dimples in the tensile fracture surface of the FSW joint, indicating that the tensile specimen of FSW is in a typical ductile fracture mode. Figure 13(a) shows the macroscopic morphology of the fracture which shows clear surface ripples. Figures 13(b−f) show SEM maps of fracture surface in the middle of the joints. It can be seen that the fracture surface in the middle of the weld is dominated by small and shallow dimples with a size of ~1 μm. Since the dimple size is related to the average grain size of the corresponding area, the dimple size is relatively small. In addition, a few large and deep dimples with obvious tearing edges on their sidewall can be seen in Fig. 13(f). This may be because the boundary between the precipitated phase particles and the surrounding matrix is prone to stress concentration and becomes the source of cracks resulting in a few large dimples. As a whole, the FSW joint has good ductility, as shown in Fig. 10(b).

Figure 14 shows the fracture morphology of the UVeFSW joint. It can be seen that there are

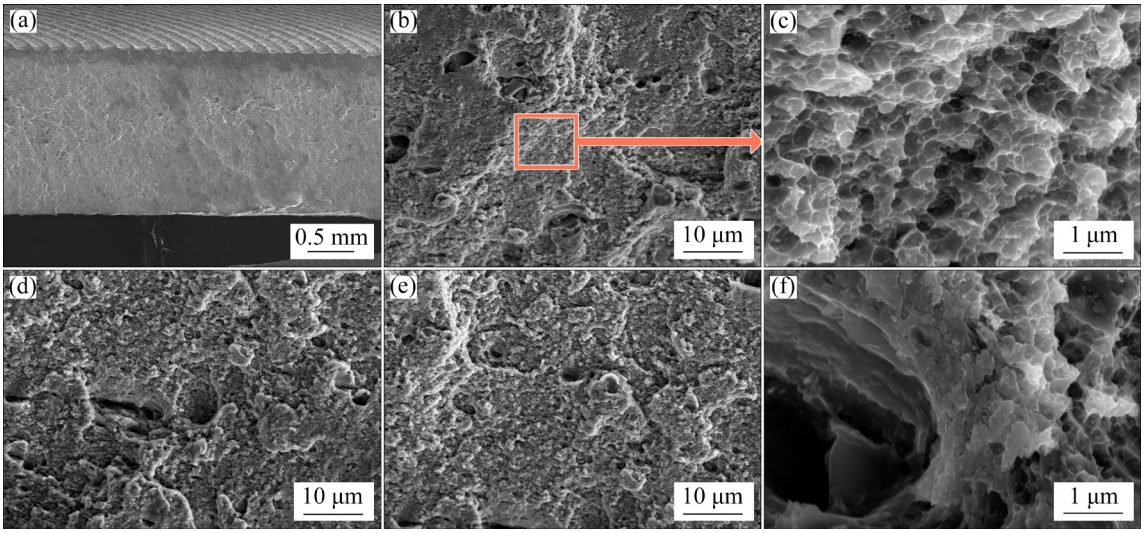

Fig. 13 Fracture surface morphologies of FSW joint obtained at welding speed of 120 mm/min: (a) Low magnification morphology of fracture surface; (b−f) High magnification morphologies of fracture surface in middle of weld

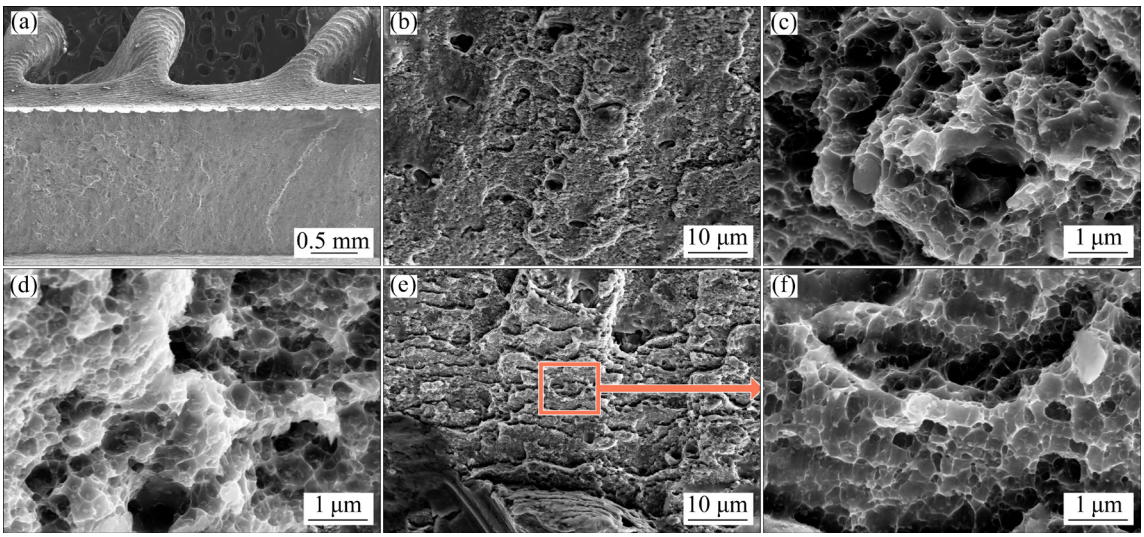

Fig. 14 Fracture surface morphologies of UVeFSW joint obtained at welding speed of 120 mm/min: (a) Low magnification morphology of fracture surface; (b−d) High magnification morphologies of fracture surface in middle of weld; (e, f) High magnification morphologies of fracture surface in bottom of weld

many small and shallow dimples in the fracture surface of the UVeFSW joint which is similar to that of the conventional FSW joint. Based on the macroscopic and microscopic features, the tensile fracture of the UVeFSW specimens is in the typical ductile fracture mode. By comparing Fig. 13(c) with Fig. 14(c), it can be seen that the depth of the dimples in the fracture surface of UVeFSW is larger, which indicates better toughness. In addition, the number of local large-sized dimples in the fracture surface of the UVeFSW is less than that in the conventional FSW joint. Figures 14(e, f) show the fracture surface morphologies at the bottom of the weld, which depicts obvious layered features with a few small dimples and many facets indicating poor toughness at the bottom of the weld.

4 Conclusions

(1) Superimposing ultrasonic vibration in FSW can improve the joint properties of 2195-T6 Al−Li alloy. The ultimate tensile strength of the conventional FSW joints at the welding speed of 570 mm/min is 390.7 MPa, while it increases to 426.8 MPa when superimposing the ultrasonic vibration in the UVeFSW.

(2) The tensile strength of UVeFSW joints increases with an increase in welding speed from 60 to 120 mm/min and then decreases with a further increase in welding speed to 570 mm/min. The maximum tensile strength of the UVeFSW joint is 449.5 MPa, which is 83.1% that of the base material.

(3) UVeFSW can suppress the welding defects which are apt to occur in the conventional FSW joints at high welding speeds. UVeFSW can significantly increase the critical welding speed and welding efficiency, while ensuring that the tensile strength of the joint is higher than 75% that of the base material.

(4) Superimposing ultrasonic vibration in FSW can enhance the recrystallization process in the WNZ of the 2195 Al−Li alloy FSW joints and increase the hardness values of the joints. The elongation of the UVeFSW joint is higher than that of the FSW joint with the same welding parameter.

CRediT authorship contribution statement

Xiang DAI: Investigation, Experiments, Software, Visualization, Data curation, Writing − Original draft; **Lei SHI:** Conceptualization, Software, Data curation, Formal analysis, Supervision, Project administration, Funding acquisition, Resources, Writing − Review & editing; **Chun-yan TIAN**: Investigation, Visualization, Formal analysis, Data curation, Writing − Review & editing; **Chuan-song WU:** Validation, Formal analysis, Funding acquisition; **Song GAO:** Validation, Formal analysis.

Declaration of competing interest

The authors declare that they have no known competing financial interests or personal relationships that could have appeared to influence the work reported in this paper.

Acknowledgments

This work was supported by the National Natural Science Foundation of China (Nos. 51905309, 52035005, 52275349); the State Key Laboratory of Solidification Processing, China (No. SKLSP201912).

References

[1] STEUWER A, DUMONT M, ALTENKIRCH J, BIROSCA S, DESCHAMPS A, PRANGNELL P B, WITHERS P J. A combined approach to microstructure mapping of an Al−Li AA2199 friction stir weld [J]. Acta Materialia, 2011, 59: 3002−3011.

[2] NAYAN N, MURTY S V S N, JHA A K, PANT B, SHARMA S C, GEORGE K M, SASTRY G V S. Mechanical properties of aluminium−copper−lithium alloy AA2195 at cryogenic temperatures [J]. Materials & Design, 2014, 58: 445−450.

[3] TAO Y, ZHANG Z, YU B H, XUE P, NI D R, XIAO B L, MA Z Y. Friction stir welding of 2060-T8 Al Li alloy. Part I: Microstructure evolution mechanism and mechanical properties [J]. Materials Characterization, 2020, 168: 110524.

[4] MISHRA R S, MA Z Y. Friction stir welding and processing [J]. Materials Science and Engineering R, 2005, 50(1/2): 1−78.

[5] XU Wei-feng, MA Jun, WANG Miao, LU Hong-jian, LUO Yu-xuan. Effect of cooling conditions on corrosion resistance of friction stir welded 2219-T62 aluminum alloy thick plate joint [J]. Transactions of Nonferrous Metals Society of China, 2020, 30(6): 1491−1499.

[6] DING Tian, YAN Hong-ge, CHEN Ji-hua, XIA Wei-jun, SU Bin. Effect of welding speed on microstructure and mechanical properties of Al−Mg−Mn−Zr−Ti alloy sheet during friction stir welding [J]. Transactions of Nonferrous Metals Society of China, 2021, 31(12): 3626−3642.

[7] XU Nan, ZHANG Wei-da, CAI Si-qi, ZHUO Yue, SONG Qi-ning, BAO Ye-feng. Microstructure and tensile properties of rapid-cooling friction-stir-welded AZ31B Mg alloy along thickness direction [J]. Transactions of Nonferrous Metals Society of China, 2020, 30(12): 3254−3262.

[8] LIU Xiao-chao, ZHEN Yun-qian, SUN Yu-feng, SHEN Zhi-kang, CHEN Hai-yan, GUO Wei, LI Wen-ya. Local inhomogeneity of mechanical properties in stir zone of friction stir welded AA1050 aluminum alloy [J]. Transactions of Nonferrous Metals Society of China, 2020, 30(9): 2369−2380.

[9] THREADGILL P L, LEONARD A J, SHERCLIFF H R, WITHERS P J. Friction stir welding of aluminium alloys [J]. International Materials Reviews, 2009, 54(2): 49−93.

[10] MENG Qiang, LIU Yang, KANG Ju, FU Rui-dong, GUO Xiao-yan, LI Yi-jun. Effect of precipitate evolution on corrosion behavior of friction stir welded joints of AA2060-T8 alloy [J]. Transactions of Nonferrous Metals Society of China, 2019, 29(4): 701−709.

[11] COLLIGAN K. Material flow behavior during friction stir welding of aluminum [J]. Welding Journal, 1999, 78(7): 229−237.

[12] ZHANG H W, ZHANG Z, CHEN J T. 3D modeling of material flow in friction stir welding under different process parameters [J]. Journal of Materials Processing Technology, 2007, 183: 62−70.

[13] ABBASI M, BAGHERI B, SHARIFI F. Simulation and experimental study of dynamic recrystallization process during friction stir vibration welding of magnesium alloys [J]. Transactions of Nonferrous Metals Society of China, 2021, 31(9): 2626−2650.

[14] GAO Chong, ZHU Zhi-xiong, HAN Jian, LI Hui-jun. Correlation of microstructure and mechanical properties in friction stir welded 2198-T8 Al−Li alloy [J]. Materials Science and Engineering A, 2015, 639: 489−499.

[15] MAO Yu-qing, KE Li-ming, LIU Fen-cheng, HUANG Chun-ping, CHEN Yu-hua, LIU Qiang. Effect of welding parameters on microstructure and mechanical properties of friction stir welded joints of 2060 aluminum lithium alloy [J]. The International Journal of Advanced Manufacturing Technology, 2015, 81(5): 1419−1431.

[16] CISKO A R, JORDON J B, AMARO R L, ALLISON P G, WLODARSKI J S, MCCLELLAND Z B, GARCIA L, RUSHING T W. A parametric investigation on friction stir welding of Al−Li 2099 [J]. Materials and Manufacturing Processes, 2020, 35(10): 1069−1076.

[17] ZHANG J, FENG X S, GAO J S, HUANG H, MA Z Q, GUO L J. Effects of welding parameters and post-heat treatment on mechanical properties of friction stir welded AA2195-T8 Al−Li alloy [J]. Journal of Materials Science & Technology, 2018, 34(1): 219−227.

[18] LI Wen-ya, JIANG Ruo-rong, ZHANG Zhi-han, MA Yu-e. Effect of rotation speed to welding speed ratio on microstructure and mechanical behavior of friction stir welded Al−Li alloy joints [J]. Advanced Engineering Materials, 2013, 15(11): 1051−1058.

[19] LIU Hui-jie, HU Yan-ying, DOU Chao, SEKULIC D P. An effect of the rotation speed on microstructure and mechanical properties of the friction stir welded 2060-T8 Al−Li alloy [J]. Materials Characterization, 2017, 123: 9−19.

[20] WANG F F, LI W Y, SHEN J, HU S Y, DOS SANTOS J F. Effect of tool rotational speed on the microstructure and mechanical properties of bobbin tool friction stir welding of Al−Li alloy [J]. Materials & Design, 2015, 86: 933−940.

[21] FONDA R W, BINGERT J F, COLLIGAN K J. Development of grain structure during friction stir welding [J]. Scripta Materialia, 2004, 51: 243−248.

[22] TAYON W A, DOMACK M S, HOFFMAN E K, HALES S J. Texture evolution within the thermomechanically affected zone of an Al−Li alloy 2195 friction stir weld [J]. Metallurgical & Materials Transactions Part A, 2013, 44(11): 4906−4913.

[23] WU Yang, MAO Hua, YANG Qing-bo, ZHANG Zhi-qing. Effect of welding parameters on defects and fracture behavior of friction stir welded 2195-T8 Al−Li alloy joints [J]. Materials Science Forum, 2018, 913: 182−189.

[24] SHUKLA A K, BAESLACK W A. Study of microstructural evolution in friction-stir welded thin-sheet Al−Cu−Li alloy using transmission-electron microscopy [J]. Scripta Materialia, 2007, 56: 513−516.

[25] QIN Hai-long, ZHANG Hua, WU Hhui-qiang. The evolution of precipitation and microstructure in friction stir welded 2195-T8 Al−Li alloy [J]. Materials Science and Engineering A, 2015, 626: 322−329.

[26] FRATINI L, BUFFA G, SHIVPURI R. Mechanical and metallurgical effects of in process cooling during friction stir welding of AA7075-T6 butt joints [J]. Acta Materialia, 2010, 58: 2056−2067.

[27] FU Rui-dong, SUN Zeng-qiang, SUN Rui-cheng, LI Ying, LIU Hui-jie, LIU Lei. Improvement of weld temperature distribution and mechanical properties of 7050 aluminum alloy butt joints by submerged friction stir welding [J]. Materials & Design, 2011, 32: 4825−4831.

[28] SHARMA C, DWIVEDI D K, KUMAR P. Influence of in-process cooling on tensile behaviour of friction stir welded joints of AA7039 [J]. Materials Science and Engineering A, 2012, 556: 479−487.

[29] SATO Y S, URATA M, KOKAWA H, IKEDA K. Hall−Petch relationship in friction stir welds of equal channel angular-pressed aluminium alloys [J]. Materials Science and Engineering A, 2003, 354: 298−305.

[30] LIU H J, ZHANG H J, YU L. Effect of welding speed on microstructures and mechanical properties of underwater friction stir welded 2219 aluminum alloy [J]. Materials & Design, 2011, 32: 1548−1553.

[31] XUE P, XIAO B L, ZHANG Q, MA Z Y. Achieving friction stir welded pure copper joints with nearly equal strength to the parent metal via additional rapid cooling [J]. Scripta Materialia, 2011, 64: 1051−1054.

[32] LIU Xiao-chao, WU Chuan-song, PADHY G K. Improved weld macrosection, microstructure and mechanical properties of 2024Al-T4 butt joints in ultrasonic vibration enhanced friction stir welding [J]. Science and Technology of Welding and Joining, 2015, 20(4): 345−352.

[33] BARADARANI F, MOSTAFAPOUR A, SHALVANDI M. Effect of ultrasonic assisted friction stir welding on microstructure and mechanical properties of AZ91−C magnesium alloy [J]. Transactions of Nonferrous Metals Society of China, 2019, 29(12): 2514−2522.

[34] TARASOV S Y, RUBTSOV V E, FORTUNA S V, ELISEEV A A, CHUMAEVSKY A V, KALASHNIKOVA T A, KOLUBAEV E A. Ultrasonic-assisted aging in friction stir welding on Al−Cu−Li−Mg aluminum alloy [J]. Welding in

the World, 2017, 61(4): 679−690.
[35] HU Yan-ying, LI Jing-long, YANG Wei-qi, MA Xian-feng, LIU Hui-jie. Role of ultrasonic in synergistic strengthening of friction stir welded 2060-T8 Al−Li alloys by grain refinement and rapid nanoscale precipitation [J]. Materials Science and Engineering A, 2022, 838: 142751.
[36] ELISEEV A A, FORTUNA S V, KALASHNIKOVA T A, CHUMAEVSKII A V, KOLUBAEV E A. Structural phase evolution in ultrasonic-assisted friction stir welded 2195 aluminum alloy joints [J]. Russian Physics Journal, 2017, 60(6): 1−5.
[37] TONGNE A, DESRAYAUD C, JAHAZI M, FEULVARCH E. On material flow in friction stir welded Al alloys [J]. Journal of Materials Processing Technology, 2017, 239: 284−296.
[38] XU Sha-men, DENG Xiao-min. A study of texture patterns in friction stir welds [J]. Acta Materialia, 2008, 56: 1326−1341.
[39] SHI Lei, WU Chuan-song, LIU Xiao-chao. Modeling the effects of ultrasonic vibration on friction stir welding [J]. Journal of Materials Processing Technology, 2015, 222: 91−102.
[40] YU Peng-fei, WU Chuan-song, SHI Lei. Analysis and characterization of dynamic recrystallization and grain structure evolution in friction stir welding of aluminum plates [J]. Acta Materialia, 2021, 207: 116692.
[41] XU W F, LUO Y X, FU M W. Microstructure evolution in the conventional single side and bobbin tool friction stir welding of thick rolled 7085-T7452 aluminum alloy [J]. Materials Characterization, 2018, 138: 48−55.
[42] HU Yan-ying, LIU Hui-jie, FUJII H, USHIODA K. Effect of ultrasound on microstructure evolution of friction stir welded aluminum alloys [J]. Journal of Manufacturing Processes, 2020, 56: 362−371.
[43] PADHY G K, WU Chuan-song, GAO Song, SHI Lei. Local microstructure evolution in Al 6061-T6 friction stir weld nugget enhanced by ultrasonic vibration [J]. Materials & Design, 2016, 92: 710−723.
[44] GAO Song, WU Chuan-song, PADHY G K. Material flow, microstructure and mechanical properties of friction stir welded AA2024-T3 enhanced by ultrasonic vibrations [J]. Journal of Manufacturing Processes, 2017, 30: 385−395.
[45] SHI Lei, WU Chuan-song, GAO Song, PADHY G K. Modified constitutive equation for use in modeling the ultrasonic vibration enhanced friction stir welding process [J]. Scripta Materialia, 2016, 119: 21−26.

超声振动对 2195 铝锂合金搅拌摩擦焊接头显微组织与力学性能的影响

戴 翔[1]，石 磊[1]，田春燕[1]，武传松[1]，高 嵩[2]

1. 山东大学 材料液固结构演变与加工教育部重点实验室，济南 250061；
2. 齐鲁工业大学(山东省科学院) 机械工程学院，济南 250353

摘 要：采用新型超声振动强化搅拌摩擦焊对第三代 2195-T6 铝锂合金进行焊接，研究超声振动对接头显微组织与力学性能的影响。研究表明，超声振动强化搅拌摩擦焊能够增强塑性材料流动，进而抑制焊接缺陷，提高无缺陷接头的临界焊接速度。在保证接头抗拉强度达到母材 75%的条件下，超声振动强化搅拌摩擦焊的焊接速度和效率均高于常规搅拌摩擦焊。施加超声振动能够大幅提升较高焊接速度条件下的接头力学性能。超声振动强化搅拌摩擦焊接头的极限抗拉强度为 449.5 MPa，达到母材的 83.1%。超声振动强化搅拌摩擦焊接能够在保证接头质量的前提下提升临界焊接速度和焊接效率。

关键词：2195-T6 铝锂合金；搅拌摩擦焊；超声振动强化搅拌摩擦焊；焊接速度；晶粒结构；接头性能

(Edited by Bing YANG)